THE PENNSYLVANIA STATE UNIVERSITY
SCHREYER HONORS COLLEGE

DEPARTMENT OF VETERINARY AND BIOMEDICAL SCIENCES

THE ROLE OF IREα AND P53 IN UVB SENSITIVITY OF HUMAN KERATINOCYTES

JACK IBINSON
SPRING 2022

A thesis
submitted in partial fulfillment
of the requirements
for a baccalaureate degree
in Immunology and Infectious Disease
with honors in Immunology and Infectious Disease

Reviewed and approved* by the following:

Adam Glick
Professor of Molecular Toxicology and Carcinogenesis
Thesis Supervisor

Pamela Hankey Giblin
Professor of Immunology
Honors Adviser

* Electronic approvals are on file.

ABSTRACT

The endoplasmic reticulum (ER) is a large membrane-bound organelle in eukaryotic cells that governs protein folding, lipid synthesis, and calcium signaling throughout its extensive network of tubules. Upon an influx of misfolded proteins and external stress, cells enter a state known as ER stress as the ER becomes overwhelmed. To remedy ER stress and restore proper protein homeostasis, cells initiate the Unfolded Protein Response (UPR) with the use of three critical proteins: Activating Transcription Factor 6 (ATF6), protein kinase R (PKR)-like endoplasmic reticulum kinase (PERK), and — the subject of this thesis — Inositol-requiring enzyme 1 (IRE1α). This thesis project aims to investigate the role of IRE1α in the context of the mutant-p53 skin cancer cell response to acute UVB exposure.

p53 is a crucial tumor suppressor protein that facilitates cell cycle arrest and recruitment of DNA Damage Response (DDR) proteins to sites of DNA damage in order to prevent mutations after damaging agents. In cases of p53 mutation, the DDR becomes altered, affecting the normal response to DNA damage and providing an opportunity for cancer to develop. Considering that UVB exposure is the most common environmental risk factor for skin cancer development, the response of cells with mutant-p53 to acute UVB exposure may give new insight into the processes of skin cancer development.

Research from Glick Lab at Penn State supports a unique role of IRE1α in both the UPR and UV-induced DDR, linking IRE1α to UV-mediated responses and potential skin cancer development. Here, we used immortalized human keratinocytes as an *in vitro* model for assessing how IRE1α and p53 expression coordinate the cellular response to acute UVB exposure.

TABLE OF CONTENTS

LIST OF FIGURES

ACKNOWLEDGEMENTS

I would like to thank Dr. Adam Glick for his sound guidance and crucial support throughout my time as an undergraduate student researcher at Penn State. I additionally give my thanks to all Glick Lab members who gave their time and energy in my training, namely Jeongin Son, Saie Mogre, Fiona Chalmers, Chase Minnich, Hailey Walsh, and Christian Pacifico. My time in this lab has provided me with some of the most enlightening and fulfilling moments of my undergraduate education, and Dr. Glick and my fellow lab members are the catalysts of this amazing experience. Lastly, I thank my family, instructors, and friends who have supported and encouraged me at every step of my educational journey.

Funding was provided by the Penn State College of Agricultural Sciences Undergraduate Research Award and the 2021 Rodney A. Erickson Discovery Grant. This study is also supported by R01 CA197142 from the National Cancer Institute to Adam B. Glick and the USDA National Institute of Food and Agriculture Federal Appropriations Project PEN04772, Accession number 100993.

Chapter 1

Introduction

1.1 Overview

This introduction provides a comprehensive background on the function of the unfolded protein response (UPR) with particular emphasis on inositol-requiring enzyme 1α (IRE1α), tumor suppressor protein p53, and the UVB-induced DNA damage response. In this thesis project, experiments were conducted utilizing immortalized human keratinocyte cell lines. Cell lines were manipulated to study key cellular responses to acute doses of UVB radiation with respect to varying expression of IRE1α and p53. This thesis serves to identify critical processes of the UVB-mediated DNA damage response (DDR) involving IRE1α and p53, posing relevance to the development of UVB-induced skin cancer.

1.2 Significance

Cancer development is defined by unchecked growth and proliferation of cells, potentially leading to metastasis as cancer cells spread over time to other organs throughout the body. Human cells employ numerous homeostatic functions to ensure genome and proteome integrity to prevent cancer and subsequent metastasis, and the specific mechanisms of these cellular checkpoints remain an important area of cancer research. Environmental stressors commonly cause disruptions in homeostatic mechanisms that lead to cancer. UV radiation stands as the most prominent environmental stressors causing skin cancers such as melanoma, a highly

invasive and lethal disease developing in skin melanocytes (1). Exposure to UV radiation also causes nonmelanoma skin cancers (NMSCs) which occur in epidermal keratinocytes, including squamous cell carcinoma (SCC) and basal cell carcinoma (BCC) (2). SCC is characterized by uncontrollable growth of keratinocytes in the outer layers of the interfollicular epidermis, commonly leading to metastasis but lower rates of mortality compared to melanoma (3). In contrast, BCC involves uncontrollable growth of cells starting from hair follicle stem cells of the interfollicular epidermis, mainly causing local destruction of tissue and rarely causing metastasis (4). Considering this thesis utilized keratinocytes, the cells composing NMSCs, SCC and BCC are most relevant to our model.

Rates of specific melanoma and nonmelanoma skin cancers have increased in recent times, dependent on a variety of genetic (skin color, sex, familial history) and nongenetic (location, age, lifestyle, sun exposure) factors (5,6). Light skin pigmentation and high amounts of UV exposure act as the most significant risk factors for skin cancer development (7). To combat the increase in skin cancer rates and to improve disease outcomes, better medical treatments and prevention measures hinge on a more complete understanding of the mechanisms leading to skin cancer development from UV exposure.

From previous research, specific gene alterations have been identified as critical to skin cancer development, such as mutation of tumor suppressor gene p53, a mutation detected in nearly all SCC cases (8). After UV-induced DNA damage, genes like p53 controlling cellular growth and preventing cancer development may become damaged, altering their functions and enabling cancer development. Additionally, the Unfolded Protein Response (UPR), a signaling cascade initiated by an influx of unfolded and misfolded proteins, may also be implicated in the progression and metastasis of cancer, including skin cancers like SCC (9). Examining the

crosstalk between tumor suppressor proteins like p53 and key protein sensors of the UPR like IRE1α as they respond to UVB-induced DNA damage may uncover specific pathways and mechanisms that determine cancer development and outcome, providing new targets for therapies and diagnostics.

1.3 The Endoplasmic Reticulum (ER)

The endoplasmic reticulum (ER) is among the most extensive and dynamic organelles found in eukaryotic cells (10). A structure of tubules spanning throughout the majority of the cell's interior, the ER is a critical membrane-bound organelle responsible for lipid synthesis and calcium signaling in its smooth portion as well as protein folding and protein synthesis in its rough portion (11). In the rough ER, ribosomes embedded in the ER membrane translate mRNA into secretory, integral, and luminal-resident proteins (12). The ER also possesses machinery aiding in the transport and trafficking of these proteins, enabling secretion of newly synthesized proteins to the cell surface or to other organelle destinations (13). The protein folding function of the ER presents particular importance for cellular homeostasis. After entering the ER, newly synthesized proteins undergo a series of modifications mediated by molecular chaperone proteins and folding enzymes to adopt their proper protein shape necessary for their functions (14). Cellular homeostasis and survival require proper protein folding as accumulation of misfolded proteins stops proper cellular functions, leading to cytotoxicity and cell death (15).

1.4 ER Stress and Proteins of the Unfolded Protein Response (UPR)

The ER sustains cell survival during periods of intense environmental and internal stress where massive accumulation of misfolded proteins occurs, a state known as ER stress (16). ER stress results from many cellular challenges, such as increased amounts of protein synthesis, impaired proteasomal degradation, inflammation, and altered calcium homeostasis (17). In response to ER stress, the ER activates a protective signaling cascade known as the Unfolded Protein Response (UPR), thereby increasing protein folding capacity of the ER, decreasing protein translation, and mediating the degradation of misfolded proteins to restore protein homeostasis (18). While periods of moderate ER stress activate the UPR to facilitate cellular repair and survival, prolonged ER stress often leads to apoptosis (19).

The UPR consists of three major transmembrane sensor proteins, each responsible for a branch of the UPR that mediates the cellular response to ER stress: PERK, ATF6, and IRE1α. First, PERK functions as a protein translational control point by phosphorylating the α subunit of translation initiation factor 2α (eIF2α), thereby activating eIF2α to reduce the formation of translation initiation complexes which in turn reduces protein translation and protein folding load (20). PERK may also help to initiate apoptosis as activated eIF2α inhibits the translation of most all mRNAs while allowing translation of a few others, including ATF4 (21). ATF4 then regulates expression of CHOP, a protein which facilitates ER stress-mediated apoptosis (21). Second, ATF6 acts as a transcription factor after being cleaved into ATF6α and ATF6β by site-1 protease (S1P) and S2P (22). ATF6α directly upregulates the expression of UPR mediator proteins such as chaperone proteins, immunoglobulin-binding protein (BiP), and X-box binding protein 1 (Xbp1) to reduce ER stress (22). Third, IRE1α activates its endoribonuclease (RNase) functionality via autophosphorylation in response to ER stress (22). The IRE1α RNase activity

then functions primarily to remove a 21-nucleotide sequence of Xbp1 mRNA, leading to the active transcription factor Xbp1s that directly enters the nucleus to alter UPR gene expression (20). IRE1α serves as the main protein of interest for this thesis project.

IRE1α possesses an N-terminal luminal domain as well as a cytosolic protein kinase and a cytosolic Rnase domain (23). Upon accumulation of misfolded proteins at the ER, BiP dissociates from the IRE1α N-terminal domain to bind to misfolded proteins, allowing IRE1α to oligomerize (23). The kinase domain of IRE1α then functions in its autophosphorylation after oligomerization, thereby activating the protein for increased Rnase activity in a back-to-back conformation (24). The active Rnase domain of IRE1α splices Xbp1 into its transcriptionally active form Xbp1s (17). Xbp1s then enters the nucleus to act as a transcription factor by binding to DNA and altering the expression of a variety of genes, including chaperone proteins and proteins involved in ER-associated protein degradation (ERAD) pathway, the pathway of the UPR that mediates protein degradation to eliminate the influx of misfolded proteins from ER stress (25). In addition to regulating Xbp1, the IRE1α Rnase domain functions in reducing the strain of protein folding on the ER through degradation of various mRNAs, a process known as regulated IRE1α-dependent decay (RIDD) (26). Lastly, IRE1α mediates cell death in times of prolonged ER stress via activating TRAF2 to interact with c-Jun amino N-terminal kinase (JNK) and ASK1 proteins, inducing pro-apoptotic signals (27).

Of note, ER stress and corresponding mediators of the UPR may play essential roles in the development of cancer. UPR molecules, particularly those mediated by IRE1α, have been identified as crucial to tumorigenesis in mounting anti-apoptotic responses that prolong survival of DNA-damaged cells and allow cancer to manifest (28). Activities of the UPR during ER stress have specifically demonstrated this inhibition of apoptosis by disrupting the anti-tumorigenic

activities of tumor suppressor protein p53 (29). The activities of p53 in response to DNA damage and in cell fate determination are critically relevant to this thesis project.

1.5 p53 and the DNA Damage Response (DDR)

A great variety of agents may cause DNA damage in cells to provoke a state of genotoxic stress. To repair DNA damage and prevent uncontrollable cell growth, cells must possess control mechanisms that result in either the survival and renewal of proper cell function or in the controlled destruction of malfunctioning cells. The DNA damage response (DDR) encapsulates signal-transduction pathways in which the cell senses and responds to DNA damage checkpoints, initiating a multitude of effector functions such as recruitment of DNA repair machinery, inhibition of the cell cycle, transcription of genes involved in the response to DNA damage, and induction of genes that trigger apoptosis (30). When a typical sequence of DNA becomes damaged through replication errors or stress from an outside agent, the cell senses DNA damage and halts its replication cycle through a series of checkpoint proteins that arrest the cell in cell cycle phase transitions, namely at the G0/G1 point, G1/S point (before DNA replication), S/G2 point, and G2/M point (before mitotic cell division) (31). Several biomarkers are rapidly induced upon activation of the DDR, including γH2AX, a protein that becomes phosphorylated to initiate downstream DDR mechanisms (32).

Furthermore, important genes known as tumor suppressor genes encode for proteins that function to arrest cell cycle progression or initiate apoptosis in the DDR (30). Proteins of these tumor suppressor genes, including retinoblastoma (Rb), Wilm's tumor (WT-1), neurofibromatosis type 1 (NF1), and p53, act to inhibit cell growth and cell proliferation at

critical cell cycle checkpoints, thus preventing tumorigenesis (33). When the DNA sequences of these tumor suppressor genes become altered, the mutant genes may lose their normal function (loss-of-function) or gain new function (gain-of-function), causing a major loss of normal cell cycle control and providing an opportunity for cancer to develop (34).

In particular, mutation of the tumor suppressor protein p53 is the most common mutation found among human cancer cells (35). p53 becomes activated by DNA damage through its acidic activation domain on its N-terminus, subsequently entering the nucleus to act as a transcription factor and upregulate the expression of several genes with upstream p53 regulatory binding domains (36). Certain covalent modifications of p53 residues by sensors of DNA damage alter p53 activity, including phosphorylation, acetylation, and methylation which enhance p53 activity, and ubiquitylation which dampens p53 activity (37). To carry out its inhibitory function on the cell cycle, activated p53 binds to the p21 promoter to upregulate the expression of p21; higher levels of p21 then function to bind and inhibit cyclin E/Cdk2 and cyclin D/Cdk4 complexes, thereby arresting cells at the G1/S phase (38).

Loss-of-function p53 mutations are strongly associated with many types of human cancers, including skin cancer (39). When the DNA sequences encoding for key p53 domains become damaged and lose function via missense mutations, the protein loses its tumor suppressor function by failing to properly regulate gene expression. Loss-of-function p53 may therefore result in an inability to halt cell cycle progression or induce apoptosis via the DDR and downstream effectors (39). Conversely, accumulation of DNA damage on the gene encoding p53 may result in gain-of-function mutations, endowing mutant p53 with a host of new capabilities that may support tumorigenesis and run against cellular anticancer mechanisms (40).

Additionally, recent preliminary data suggests that p53 is recruited to sites of DNA damage within seconds of UV-irradiation, serving as a crucial sensor for DDR pathways (41). The exact mechanisms and functions of p53 activation in response to DNA damage and upregulation of DDR-related genes after UV exposure is the subject of ongoing research. p53 and its relationship to ER stress and UVB-induced DDR is of particular importance for this thesis.

1.6 UVB-induced DDR

As previously mentioned, UV radiation may cause severe damage to cells, impairing their normal cell functions. UVA and UVB rays from the nuclear fusion reaction of the sun may penetrate through the atmosphere and damage exposed skin cells (42). UVB radiation (wavelength of 280-315 nm) is often considered more carcinogenic than UVA radiation (wavelength of 315-400 nm) as it is absorbed more by DNA, thus the effects of UVB radiation on DNA integrity is commonly studied in cancer research (42). High doses of UVB radiation cause two distinct types of DNA damage: the more frequent cyclobutane pyrimidine dimers (CPDs), a type of DNA damage in which adjacent pyrimidine bases on the same strand of DNA bind with each other to form a four-membered ring, and the less frequent pyrimidine-pyrimidone 6-4 photoproducts (6-4PPs), a DNA instability where two adjacent pyrimidine bases on the same strand of DNA bind to form an oxetane structure (43). Cancer research primarily focuses on the DDR mechanisms for repairing CPDs as opposed to 6-4PPs because CPDs are believed to be the dominant contributors of UVB-induced mutations in mammalian skin cells (44).

To respond to UV-induced DNA damage, cells employ many of the same mechanisms as previously discussed in the DDR. In particular, tumor suppressor protein p53 has been observed to mediate key protective responses of UV-induced DDR (45). In the presence of CPDs, p53 activation induces either apoptosis or cell cycle arrest and repair, serving as a crucial regulator for DDR pathways in response to UV-induced damage (46). Additionally, activated caspase-3 has been upregulated in UVB-induced apoptosis of human keratinocyte skin cells *in vitro* (47). Caspase-3 activation through cleavage has been identified as a typical hallmark for apoptosis, thus posing particular importance to UVB-induced cell death (48).

Historically, UVB radiation is known to cause the majority of sunlight-induced cancers (49). Environmental stressors such as UVB have been further observed to induce states of ER stress, activating IRE1α in its UPR and ERAD functions to protect against DNA damage and sustain survival (50). As previously mentioned, the mechanisms of ER stress may function to disrupt the tumor suppressor activities of p53 (29). IRE1α may therefore pose significance in the context of clearing ER stress to allow for proper p53 tumor suppressor function to prevent UVB-induced skin cancer.

1.7 Aim of This Study

Recent experiments from our researchers at the Glick Lab identify IRE1α activation as a key component of the UV-induced DDR by regulating reactive oxygen species (ROS), controlling ER calcium efflux, and inducing the expression of proteins involved DNA repair responses such as cleaved Caspase-3 and γH2AX (51). The aim of this experiment is to further

investigate the effect of IRE1α expression on UVB sensitization of human keratinocytes *in vitro* with an added focus on tumor suppressor protein p53.

For the mutant p53 model, HaCaT cells were utilized. HaCaT cells are an immortalized human keratinocyte cell line that possess a mutant p53 spectrum consistent with UVB-induced damage (52). HaCaT cells have also been utilized as reliable models for testing inflammatory and repair responses of human keratinocytes (53). For the wildtype p53 model, N-TERT cells were employed. Similar to HaCaT cells, N-TERT cells are an immortalized human keratinocyte cell line that serve as a suitable model for human skin responses (54). Knockdown, control, and overexpression IRE1α lines were generated in both HaCaT and N-TERT cells via lentivirus transduction. Protein knockdown and overexpression was confirmed by Western Blotting.

To assess cellular responses following UVB irradiation, cell staining was utilized to quantify cleaved Caspase-3, a crucial biomarker of apoptosis, as well as basal calcium homeostasis with respect to p53 and IRE1α expression in the cell lines. Immunofluorescence was also used to assess levels of γH2AX, a hallmark of DNA damage. To determine cell survival after UVB irradiation, MTT colorimetric assay was used, a prominent assay for quantifying cell viability after treatment with various agents (55). In all, these *in vitro* experiments illustrate the role of p53 and IRE1α in the UVB-induced DNA damage response of human keratinocyte skin cells, posing particular importance to the mechanisms of skin cancer.

Chapter 2

Materials and Methods

2.1 HaCaT and N-TERT Cell Culture

HaCaT and N-TERT cells were grown to confluence in 60 mm standard tissue culture dishes at 10% CO2 and 37 ºC. HaCaT cells were grown in 4 mL of EMEM Cell Culture Medium (Ca^{2+} free EMEM, 10% FBS, 1% Pen/Strep Antibiotic) (VWR 06-174G), and N-TERT cells were grown in 4 mL of serum-free Cascade Biologics Medium 154 (GIBCO M-154-500) with added KGM-2 SingleQuots Keratinocyte Growth Factors (LONZA CC-4152). The KGM-2 SingleQuots kit contains growth factors, cytokines, and other supplements to encourage optimal cell growth of keratinocytes in a serum-free environment, including: bovine pituitary extract (BPE), human epidermal growth factor (HEGF), Recombinant human insulin (0.5%), hydrocortisone, transferrin, epinephrine, and gentamicin sulfate-Amphotericin (GA-1000). Cell culture media was changed every other day.

Cells were passaged at 1:5 dilution after reaching confluence. In passaging, cells were first aspirated and washed twice with sterile 1X PBS. Cells were then trypsinized with 2 mL of trypsin + EDTA for 15 minutes at 37 ºC. To trypsinized HaCaT cells, 2 mL of Low Calcium EMEM culture media was used to neutralize trypsin, then all 4 mL of cell mixture was collected and spun down at 800 rpm for 5 minutes. HaCaT cells were then aspirated and resuspended in 5 mL of Low Calcium EMEM culture media. 1 mL of cell suspension was added to a new 60 mm dish containing 3 mL of Low Calcium EMEM culture media to complete passaging. To trypsinized N-TERT cells, 2 mL of N-TERT cell media (DMEM, 5% heat inactivated FBS, 1% Pen/Strep Antibiotic) (Corning 10-017-CV) was used to neutralize trypsin, then all 4 mL of cell

culture mixture was collected and spun down at 800 rpm for 5 minutes. N-TERT cells were then aspirated and resuspended in 4 mL of sterile 1X PBS to wash out all serum, and the mixture was spun down again at 800 rpm for 5 minutes. N-TERT cells were subsequently aspirated and resuspended in 5 mL of Cascade Biologics Medium 154 + Keratinocyte Growth Factors culture medium. 1 mL of cell suspension was added to a new 60 mm dish containing 3 mL of Cascade Biologics Medium 154 + Keratinocyte Growth Factors culture medium to complete passaging. In plating cells for UV irradiation experiments, a CytoSMART Corning Cell Counter was utilized to calculate effective dilutions for ensuring equal plating of cells.

2.2 Lentivirus Transduction

To generate lentivirus vectors expressing IRE1α mutants, HEK293T cells were cotransfected via Lipofectamine 3000 (ThermoFisher L3000015). In 10 cm cell culture dishes, $5x10^6$ HEK293T cells were seeded in each dish in 10 ml of HEK293T growth media (DMEM + Glucose + L-glutamine, 1X non-essential amino acids, 10% FBS, 1mm Sodium Pyruvate , 0.75mg/ml Sodium bicarbonate , 10mm HEPES , 1% Pen/Strep antibiotic). Upon reaching 60% confluence, HEK293T cells underwent transfection. The vector/P3000 enhancer mixture was prepared by mixing psPAX2, pMD2.G, and pCW57.1-IRE1α WT/Mutant in a 1:1:2 molar ratio with P3000 enhancer in SFAF DMEM cell culture medium (DMEM + Glucose + L-glutamine, 1X non-essential amino acids, 1mm Sodium Pyruvate, 0.75mg/ml Sodium bicarbonate, 10mm HEPES). pCW57.1-IRE1α WT/Mutant expression vector was generated by Dr. Jeongin Son and Saie Mogre. The vector/P3000 enhancer mixture was mixed with a Lipofectamine 3000/SFAF cell culture medium mixture, subsequently being added dropwise to the HEK293T cells. After 16

hours, the transfection media was aspirated and replaced with HEK293T growth media. At 48 and 96 hours after replacing the transfection media, lentivirus-containing supernatant was collected as media was draw off into conical tubes, spinning down at 2000 rpm for 5 minutes at room temperature. The lentivirus was finally concentrated by adding 1X PEG, a dilution of 4X PEG (40g of PEG 6000 in 75ml of nanopore water containing 2.5M NaCl).

To generate IRE1α knockdown, control, and overexpression lines of HaCaT and N-TERT cells, cells were first plated into 6-well cell culture plates with 2 mL of culture media per well, 3 wells for HaCaT and 3 wells for N-TERT. Upon reaching 70% confluence, cells were aspirated, and transduction media was applied to each well, consisting of 2 mL of culture media, 16 μl of Polybrene solution, and a volume of corresponding lentivirus that yielded a multiplicity of infection (MOI) of 100. For both HaCaT and N-TERT, 1 well received shCtrl lentivirus while 2 wells received shIRE1α lentivirus. Cells were then incubated at 37 ^{o}C while rocking overnight to allow for lentivirus transduction of shIRE1α or shCtrl lentiviruses. Afterwards, cells were aspirated, and new culture media was applied to allow cells to recover for one day. Then, cells underwent puromycin selection as media was changed with added puromycin (VWR 540222) to select for only virus-infected cells containing the puromycin resistance gene. After selection, 1 well of each HaCaT and N-TERT shIRE1α transduced cells underwent lentivirus transduction a second time with dox-inducible hIRE1α, following the same procedure. Following puromycin selection, shCtrl (control), shIRE1α (knockdown), and shIRE1α + dox-inducible hRE1α (overexpression) lines were successfully generated in the HaCaT and N-TERT cell types as confirmed by Western Blotting.

2.3 siRNA Transfection

To obtain p53 knockdown, HaCaT and N-TERT cell lines underwent siRNA transfection with either ON-Targetplus siRNA SMARTpool human p53 siRNA (Horizon L-003329-00-0010) or siCtrl. The SMARTpool siRNA combines 4 gene-specific siRNA to yield greater knockdown efficiency of target mRNA p53 and fewer off-target effects on unintended mRNA molecules. siCtrl is a randomly scrambled sequence that yields no specific mRNA degradation, thus serving as a control for siRNA transfection. Upon reaching 70% confluence in a 6-well plate, cells were treated with transfection media containing siRNA at 25 nM concentration diluted from 50 μM stock. The proper volume of each siRNA (siCtrl and sip53) was added in a 1:6 ratio to tubes with P3000 Chelator (Life technologies L3000-015) and cell culture media, incubating at room temperature for 5 minutes. Simultaneously, Lipo3000 was mixed in a tube containing cell culture media, incubating at room temperature for 5 minutes. After incubation, half of the Lipo3000 mixture was mixed dropwise to each siRNA mixture tube, incubating for 15 minutes at room temperature to generate siRNA-lipid transfection complexes. Media containing siRNA-transfection complexes was then added dropwise onto the cells, swirling occasionally, and allowing to incubate at 37 ^{o}C for 6 hours. After incubation, the cells were aspirated, and fresh cell culture media was applied. Effective p53 knockdown occurs 3-5 days post transfection. 1 day post-transfection, cells were passaged to 96-well plates. 3 days post-transfection, UV treatment was applied to cells.

2.4 UVB Irradiation

To administer acute doses of UVB (280-315 nm) radiation to cells, a CL-1000 Ultraviolet crosslinker was utilized. 24 hours before treatment, hIRE1α overexpressing cells were treated

with 500 ng/mL of doxycycline to induce IRE1α expression. Before treatment, cell media was drawn off into separate tubes and spun down at 800 rpm for 5 minutes. Sterile 1X PBS was applied to each well. UVB radiation doses were applied to each designated well of cells, covering all other wells with tin foil to shield from UVB radiation. PBS was aspirated from each well after UVB irradiation, and the spun down media was reapplied to the cells. Cells were incubated until appropriate time points for analysis.

2.5 Protein Isolation and Western Blot Analysis

After treatment with UVB radiation, cells were harvested to extract proteins. Cells were first washed twice with ice cold PBS, then RIPA lysis buffer (50mM Tris- HCl, pH 7.4, 150 mM NaCl, 1% IGEPAL, 0.5% Sodium Deoxycholate, 0.1% SDS, 2 mM EDTA, 2 mM beta-glycerophosphate, 5 mM NaF, 1 mM PMSF, 1 μg/mL Aprotinin, 5 μg/mL Leupeptin, 1 μg/mL Pepstatin, and 2 mM Sodium Orthovanadate) was applied to lyse the cells. Cells were scraped and drawn off into tubes, then each sample tube was sonicated at an amplitude of 100 for 7 seconds. Samples were centrifuged at 4 ^{o}C and 15000 rpm for 20 min. The supernatant was collected, and protein concentrations were obtained from supernatant using the BCA assay (Pierce 23225) with standards prepared from distilled water, RIPA lysis buffer, and 2mg/mL BSA. All measurements were taken in duplicates and loaded into a 96-well plate, each sample well containing 5 μl of sample with 20 μl of distilled water. 200 μl of BCA dye was added to each well (1:50 ratio of BCA reagents B:A), incubating for 30 minutes at 37 ^{o}C. Absorbances were then measured at 560 nm using a Promega GloMax-Multi Detection System, and proper amounts of sample and loading dye were calculated for each sample.

Protein samples (20μg concentrations) were run for about 120 min at 100V on SDS-PAGE gels of 10% and 15% with a PageRuler prestained protein ladder (ThermoFisher, 26619), stopping before the samples reached the end of the gels. After running a gel, a semi-wet transfer to a nitrocellulose membrane was completed using the Bio-Rad Trans-Blot TURBO Transfer System as described by the manufacturer. The membrane was then rocked in ponceau S solution (SigmaAldrich P7170) for 5 minutes and rinsed in DI water to allow for protein band visualization. Strips were cut according to the location of proteins of interest based on the protein ladder. After cutting, the strips were rocked for 65 minutes at room temperature in a blocking solution of 5% BLOTTO Milk (Rockland B501-0500) in TBST (20ml Tris pH 7.4, 40ml 5M NaCl, 4ml Tween 20, filled to 2L with dH2O). Strips were then incubated with primary antibody at 1:1000 dilution in 1% bovine serum albumin (BSA) (SigmaAldrich A7906-100G) in TBST, rocking overnight at 4 ^{o}C. The primary antibody was then drawn off, and the strips were washed by shaking three times in TBST for 10 minutes each. Secondary antibodies were then applied in 1:1000 dilution in 1% BSA in TBST, rocking for 1 hour at room temperature. After pouring off all secondary antibodies and further washing, proteins were detected using a KwikQuant Imager after application of ECL (Pierce 34094) or West PICO plus (ThermoFisher 34580) substrate.

2.6 MTT Cell Viability Assay

After treatment with UVB, MTT cell viability assays were conducted to assess UVB sensitization in each cell line at varying UV doses and time points. In MTT assays, metabolic activity is measured as oxidoreductase enzymes in the mitochondria of cells reduce yellow-colored MTT to purple-colored formazan (55). Increased formazan concentrations cause

increased absorbances, thus indicating increased cell viability. which 5 mg/ml filter-sterilized MTT (ThermoFisher M6494) in PBS was added in a 1:5 ratio to existing cell culture media on irradiated cells in a 96-well plate. Cells were left to incubate for 3 hours at 37 ºC. After being aspirated, MTT solvent (4 mM HCl, 0.1% Nondet P-40 (NP40) in isopropanol) was added to each well in amounts equal to the original cell culture media volume, and three blank wells of only MTT solvent were created. Cell plates were covered with tinfoil and shaken for 15 minutes. After shaking, absorbances of each plate was measured at 560 and 750 nm using a Promega GloMax-Multi Detection System. Calculations were made to eliminate background absorbance, and measurements for each cell line were normalized to respective control values. Statistical significance was determined by Student's t-test.

2.7 Cell Staining and Immunofluorescence

To quantify the amount of intracellular calcium and expression of apoptosis marker cleaved Caspase-3, cells were stained and visualized using fluorescent microscopy. In their existing cell culture media, cells were treated with either 5 mM of Fluo-4- acetoxymethyl ester (Fluo-4, AM) (Invitrogen F14201) for intracellular calcium staining or with 30μL/mL CellEvent Caspase-3/7 Green Detection Reagent (Invitrogen C10423) for 1 hour at 37 ºC, later nuclear counterstaining with Hoechst dye (Invitrogen H3570). Images of fields were taken for each well of cells using a BZ-9000 fluorescence microscope, 2 images per field (1 stain, 1 counterstain).

To quantify expression of γH2AX, cells were fixed in 4% paraformaldehyde and permeabilized using 1% Triton X-100 (SigmaAldrich 9036-19-5) in 1X PBS. Cells were then blocked for 1 hour at 37 ºC using 5% normal goat serum (VectorLabs S-1000-20) in PBS.

Afterwards, cells were incubated with γH2AX primary antibody at 1:1000 dilution in 1% normal goat serum in PBS, rocking overnight at 4 ^{o}C. The primary antibody was drawn off, and secondary antibody conjugated with fluophores (anti-mouse Alexa-fluor 594) (Cell Signaling Technology 8890S) was then applied in 1:1000 dilution in 1% normal goat serum in PBS, rocking for 1 hour at 37 ^{o}C. Nuclear counterstaining was then completed using Hoechst dye. Images of fields were taken for each well of cells using a BZ-9000 fluorescence microscope, 2 images per field (1 stain, 1 counterstain).

Utilizing QuPath software, total cell counts were obtained using blue field detection of Hoechst nuclear staining with a threshold of 15. For Fluo-4, AM Calcium staining, positive cells counts were obtained using a green field detection threshold of 10. For cleaved caspase-3 staining, positive cell counts were obtained using a green field detection threshold of 5. For γH2AX immunofluorescence, positive cell counts were obtained using a red field detection threshold of 5. Percentage of positive cells was obtained for each field by taking the count of positive stained cells in a given field divided by the total count of Hoechst-stained nuclei in the same field. Results were compared to determine statistical significance across cell lines. Significance was determined by Student's t-test.

Chapter 3

Results

3.1 Confirmation of IRE1α Knockdown and Overexpression in HaCaT and N-TERT Cell Lines

IRE1α knockdown (shIRE1α), control (shCtrl), and overexpression (shIRE1α+hIRE1α) cell lines were generated in HaCaT and N-TERT immortalized human keratinocytes with the help of Dr. Jeongin Son, a graduate student in the Glick Lab. To confirm IRE1α knockdown and overexpression in both HaCaT and N-TERT cells, protein samples harvested from each cell line were analyzed via Western Blotting, using β-Actin as a loading control. Figure 1 indicates that lentivirus transduction yielded effective IRE1α knockdown and overexpression in HaCaT cells as evidenced by a faint band in the shIRE1α line and an intense, smeared band in the shIRE1α+hIRE1α line, respectively. While a slight band is observable in the IRE1α region for the HaCaT shIRE1α line, this band is visibly much fainter than in the HaCaT shCtrl line, indicating successful knockdown. Figure 1 also indicates successful lentivirus transduction in N-TERT cells, yielding complete IRE1α knockdown as evidenced by no apparent band in the shIRE1α line. Figure 1 also indicates successful lentiviral transduction and overexpression of IRE1α in the N-TERT shIRE1α+hIRE1α cell line, evidenced by an intense upper band corresponding to dox-inducible exogenous hIRE1α overexpression and a faint lower band corresponding to endogenous IRE1α expression. This exogenous hIRE1α appeared higher than endogenous IRE1α as exogenous hIRE1α contains a Myc tag, making the protein larger by about 1.2 kDa.

Figure 1. Western Blot of HaCaT and N-TERT cell lines

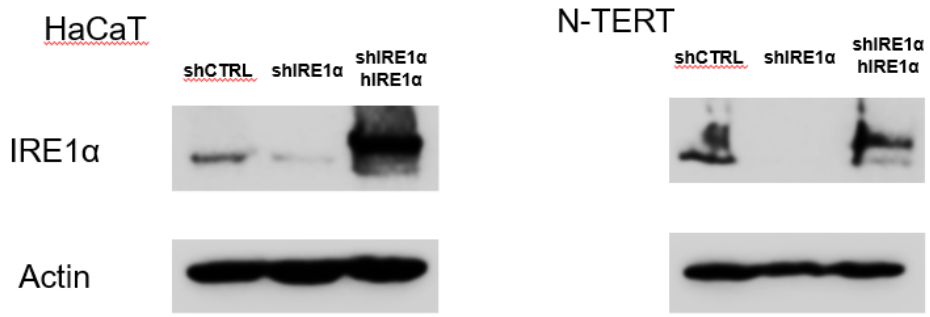

Western Blot analysis of IRE1α and β-Actin (loading control) in shCtrl, shIRE1α, and shIRE1α+hIRE1α lines of HaCaT and N-TERT human keratinocytes. β-Actin intensity is consistent across each sample, indicating proper protein loading. Relative band intensities correspond to relative protein concentration. In IRE1α, upper band corresponds to exogenous hIRE1α and lower band corresponds to endogenous IRE1α.

3.2 hIRE1α overexpression rescues HaCaT cells from death in response to acute UVB irradiation

To assess UVB sensitivity as it relates to IRE1α expression in keratinocytes with mutant-p53 expression, a UVB dose-response MTT cell viability assay was performed in the HaCaT cell lines generated from lentivirus transduction. HaCaT cells were exposed to 35.0, 50.0, and 65.0 mJ/cm^2 doses of UVB radiation after reaching full confluency. Absorbance measurements were taken 32 hours post-UVB irradiation, and measurements were normalized to no UV control.

From Figure 2A, knockdown of IRE1α in HaCaT cells resulted in significantly decreased survival compared to control and overexpression cell lines at all doses of UVB radiation. Furthermore, Figure 2A also shows that hIRE1α overexpression in HaCaT cells resulted in increased cell survival at all doses of UVB radiation compared to IRE1α control and knockdown cell lines, thereby rescuing cells from UVB-mediated death. The most significant differences in cell viability between each of the cell lines occurred with the 35.0 mJ/cm^2 UVB dose, so this

dose was chosen for use in further HaCaT experiments. Figure 2B illustrates a negative trend in cell viability with increasing doses of UVB radiation in all of the HaCaT cell lines.

Figure 2. HaCaT UVB Dose-Response MTT Cell Viability Assay

A.

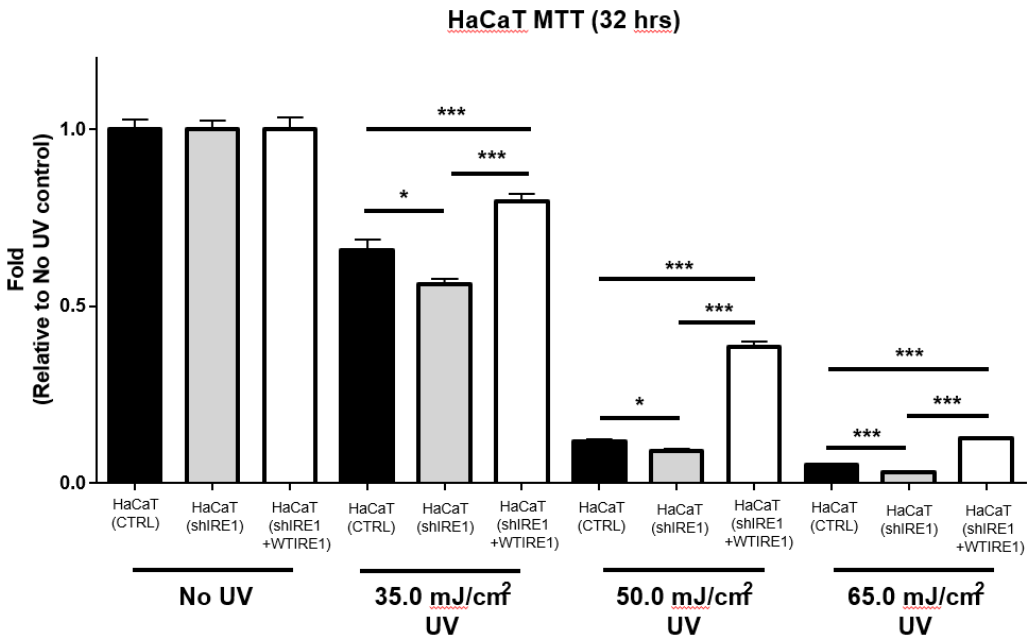

B.

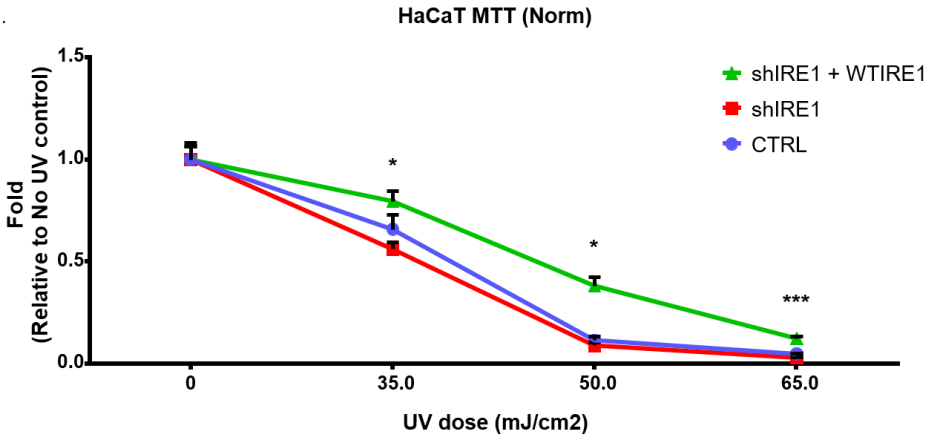

(A) MTT cell viability assay 32 hours post-UVB irradiation for each HaCaT cell line (n = 6 per line per dose) normalized to No UV control. (B) Results from MTT assay displayed as a line graph for trend determination. * = "p < 0.05", ** = "p < 0.01", * = "p < 0.001".**

3.3 Knockdown of IRE1α in HaCaT cells leads to increased cleaved Caspase-3 in response to acute UVB irradiation

As previously mentioned in the introduction, cleaved Caspase-3 serves as a key biomarker of apoptosis (48). By staining cells to measure cleaved Caspase-3 expression following UVB irradiation, an accurate measurement of apoptosis in skin cells may be obtained as a percentage of total skin cells exposed. This provides a quantitative means of measuring UVB sensitization of human skin cells *in vitro*.

To assess how IRE1α expression influences UVB-induced apoptosis in human keratinocytes with mutant p53, cleaved Caspase-3 staining was completed on the HaCaT cell lines generated from lentivirus transduction. After the cells reached full confluency, a UVB dose of 35.0 mJ/cm^2 was used as determined from the results of the previous HaCaT UVB dose-response MTT cell viability assay. Cleaved Caspase-3 staining and Hoechst nuclear counterstaining were performed 10 hours post-UVB irradiation.

From figure 3A, IRE1α knockdown in HaCaT cells resulted in significantly increased expression of cleaved Caspase-3 after UVB irradiation compared to control. Additionally, Figure 3A shows that reintroduction of hIRE1α in the overexpression line resulted in significantly decreased cleaved Caspase-3 expression following UVB irradiation as compared to knockdown IRE1α. Figure 3A also shows a nonsignificant difference in cleaved Caspase-3 expression comparing control to hIRE1α overexpression, indicating hIRE1α overexpression reverses the effect of IRE1α knockdown. Figure 3B displays representative Caspase-3 staining images for each cell line at No UV and 35.0 mJ/cm^2 UV. Taken together, these results indicate that IRE1α knockdown results in increased UVB-induced apoptosis in p53-mutant skin cells *in vitro*, and hIRE1α overexpression reverses this effect.

Figure 3. HaCaT cleaved Caspase-3 staining after UVB irradiation

A.

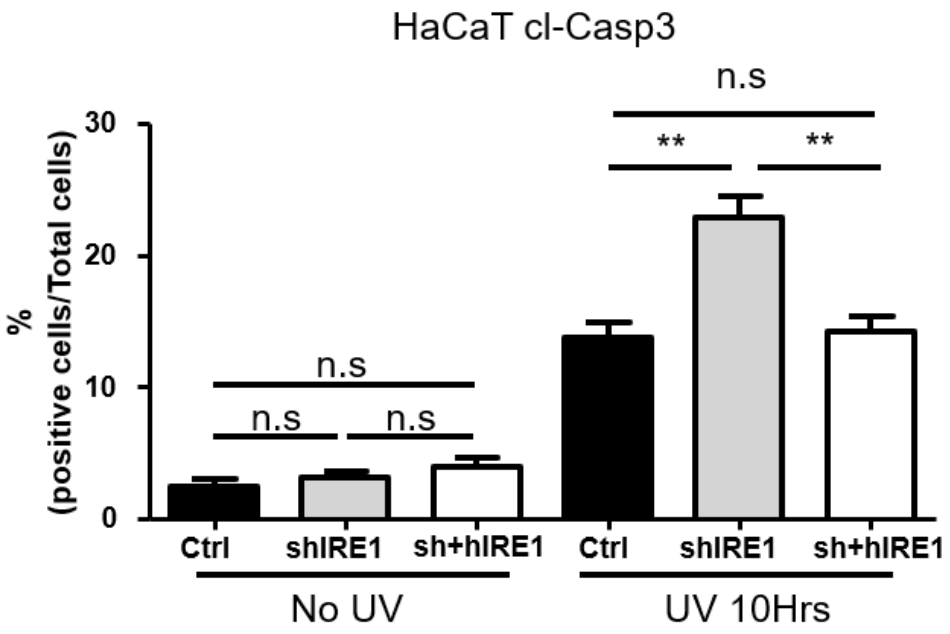

B.

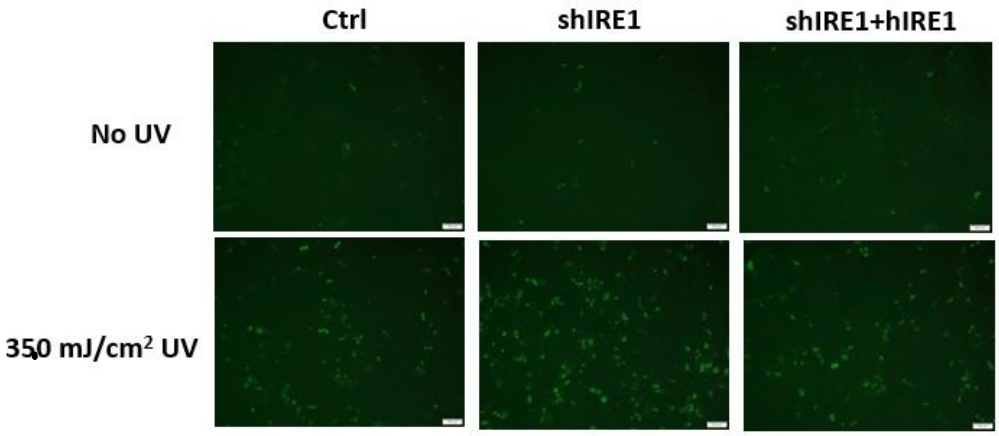

(A) Cleaved Caspase-3 staining of HaCaT cell lines 10 hours after 35.0 mJ/cm^2 dose of UVB radiation. n.s. = "no significance", ** = "p < 0.01". (B) Cell images of UVB-treated cells (n = 5 fields per cell line per dose) visualized at 20x magnification. Cells counted via QuPath Cell Imaging Software.

3.4 Basal level of calcium in HaCaT cells increases with IRE1α knockdown

ER stress is marked by a variety of imbalances in normal cell states, including altered calcium homeostasis (17). As previously mentioned, the Glick Lab has identified IRE1α as a critical protein involved in managing ER calcium efflux during times of UV-induced DDR (51).

While investigating the behavior of p53-mutant human keratinocytes, determining the effect of IRE1α expression on intracellular calcium levels may be of particular importance.

To study how IRE1α alters intracellular calcium levels in human keratinocytes with mutant p53, Fluo-4, AM Calcium staining was performed on the HaCaT cell lines generated from lentivirus transduction. After reaching full confluency, Fluo-4, AM Calcium staining and Hoechst nuclear counterstaining was performed on all HaCaT cell lines without any UVB irradiation to determine basal calcium levels.

From Figure 4A, knockdown of IRE1α resulted in significantly increased basal intracellular calcium levels in HaCaT cells compared to control and overexpression. These results support Glick Lab's previous evidence that IRE1α is essential in managing ER calcium efflux. While Figure 4A shows significantly increased basal intracellular calcium levels in hIRE1α overexpression cells compared to control, hIRE1α overexpression cells expressed significantly decreased basal intracellular calcium levels compared to IRE1α knockdown. This result indicates that hIRE1α overexpression partially, but not completely, reverses the effect of IRE1α knockdown on basal calcium levels. Figure 4B displays representative intracellular calcium staining images for each of the cell lines under basal conditions. In all, these results indicate that IRE1α knockdown in HaCaT cells yields an increase in intracellular calcium levels, supporting the notion that IRE1α plays a role in calcium efflux, potentially impacting key cellular responses including ER stress and the UV-induced DDR.

Figure 4. HaCaT cell lines basal calcium staining

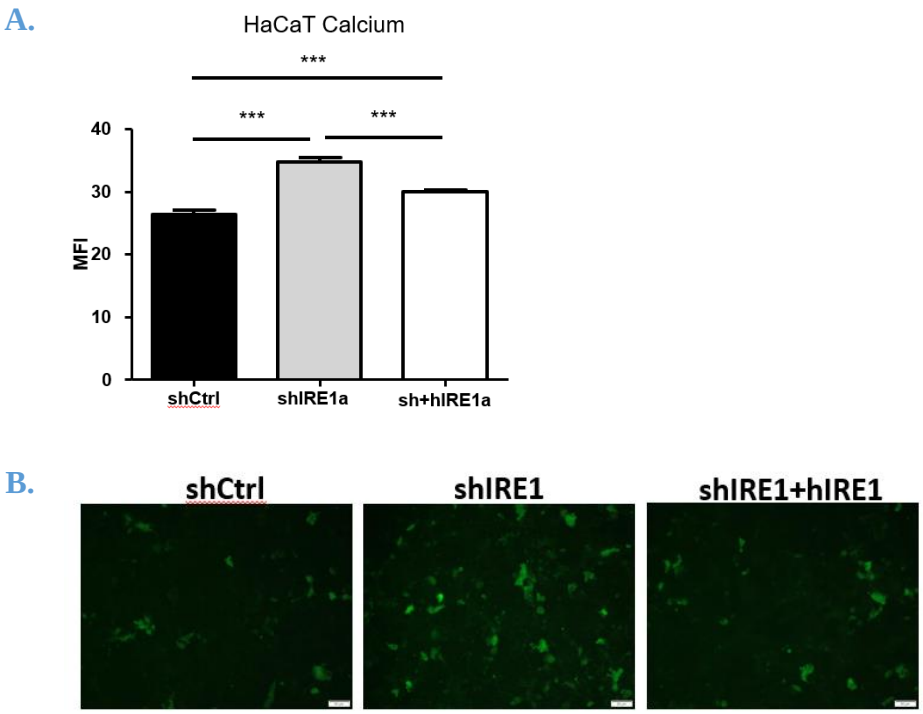

(A) Fluo-4, AM Calcium Staining of HaCaT cell lines. * = "p < 0.001". (B) Cell images of basal calcium staining (n = 9 fields per cell line) visualized at 20x magnification. Cells counted via QuPath Cell Imaging Software.**

3.5 Knockdown of IRE1α in HaCaT cells leads to decreased γH2AX expression in response to acute UVB irradiation

γH2AX serves as a key biomarker for DNA damage and the induction of the DDR (32). Downregulation of γH2AX may therefore indicate decreased cellular capability to respond to DNA damage. In the context of p53 mutant skin cells, decreased capacity to effectively recognize DNA damage leads to decreased initiation of the DDR, potentially initiating apoptosis as the cells may not repair DNA damage. To assess the effect of IRE1α on γH2AX expression after acute UVB exposure p53 mutant skin cells, γH2AX immunofluorescence was performed with the help of Dr. Jeongin Son. After reaching full confluency, the HaCaT lines generated from

lentivirus transduction were irradiated with a dose of 35.0 mJ/cm^2 UVB. Cells were fixed 6 hours post-irradiation, incubating in γH2AX primary antibody. This incubation was followed by incubation with secondary antibody conjugated with fluophores and subsequent nuclear counterstaining with Hoechst.

From Figure 5A, IRE1α knockdown in HaCaT cells resulted in significantly decreased expression of cleaved γH2AX after UVB irradiation compared to control. Figure 5A also shows that γH2AX expression after UVB irradiation was restored to control levels with dox-induced hIRE1α overexpression in HaCaT cells. Figure 5B displays representative γH2AX for each cell line at No UV and 35.0 mJ/cm^2 UV. In all, these results corroborate Glick Lab's previous findings that IRE1α knockdown leads to decreased γH2AX expression following exposure to acute doses of UVB. These results further illustrate the role of IRE1α as a regulator of the UV-induced DDR outside of its typical UPR functions in human skin cells.

Figure 5. HaCaT γH2AX immunofluorescence after UVB irradiation

A.

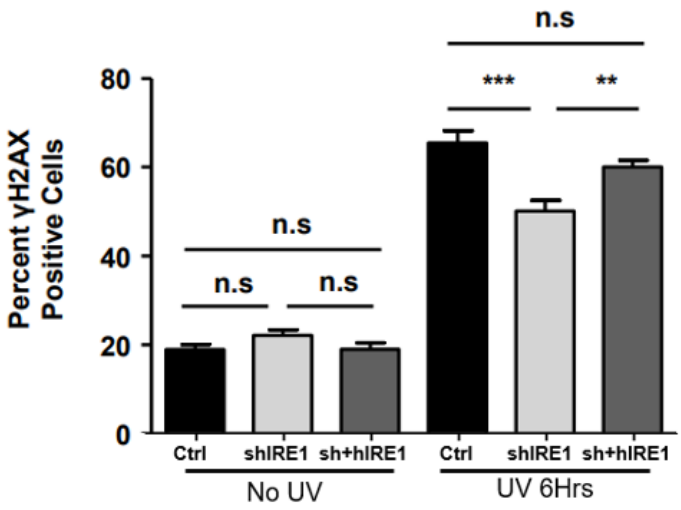

B.

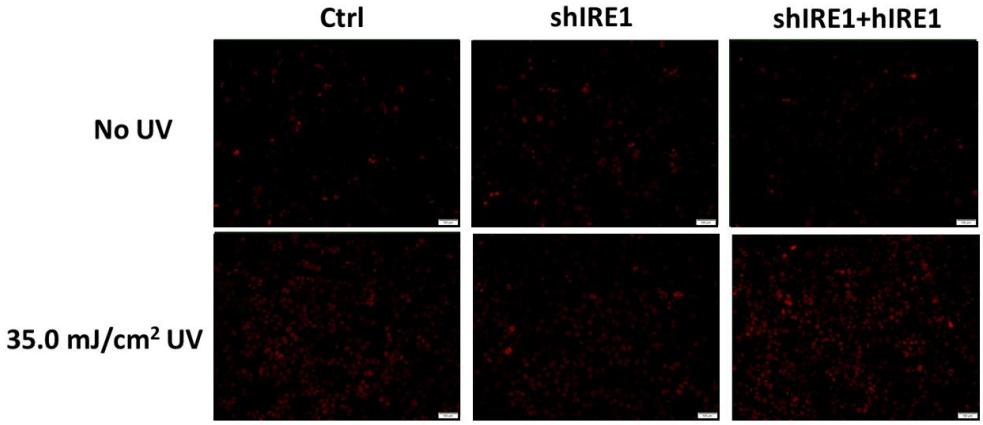

(A) γH2AX immunofluorescence of HaCaT cell lines 6 hours after 35.0 mJ/cm^2 dose of UVB radiation. ** = "p < 0.01", * = "p < 0.001", n.s. = no significance. (B) Cell images of γH2AX immunofluorescence (n = 12 fields per cell line per dose) visualized at 20x magnification. Cells counted via QuPath Cell Imaging Software.**

3.6 IRE1α knockdown rescued N-TERT cells from death in response to acute UVB irradiation

To assess how IRE1α expression affects UVB sensitivity of human keratinocytes with wildtype p53, a UVB dose-response MTT cell viability assay was again performed, this time using N-TERT cell lines generated from lentivirus transduction. This experiment utilized the

same protocol as was used for HaCaT cells, but UVB doses were adjusted to 15.0 mJ/cm^2, 35.0 mJ/cm^2, and 50.0 mJ/cm^2. Absorbance measurements were taken 24 hours post-UVB irradiation, and each measurement was normalized to no UV control.

From Figure 6A, IRE1α knockdown in N-TERT cells resulted in significantly decreased cell death compared to hIRE1α overexpression at 35.0 and 50.0 mJ/cm^2 of UVB. Additionally, Figure 6A shows that hIRE1α overexpression in N-TERT cells resulted in significantly increased cell death compared to IRE1α control at all UVB doses. Figure 6A also shows that cell death following UVB irradiation of IRE1α knockdown N-TERT cells was only significantly different compared to IRE1α control at 50.0 mJ/cm^2, the highest dose of UVB radiation, which resulted in decreased death of IRE1α knockdown cells. From Figure 6A and the trendline in Figure 6B, irradiation with 35.0 mJ/cm^2 yielded increased cell survival in IRE1α knockdown N-TERT cells compared to No UV control dose. These results indicate that IRE1α knockdown in cells with a wildtype p53 phenotype leads to decreased sensitivity to UVB radiation, rescuing cells from death.

Figure 6. N-TERT cells MTT viability assay following UVB irradiation

A.

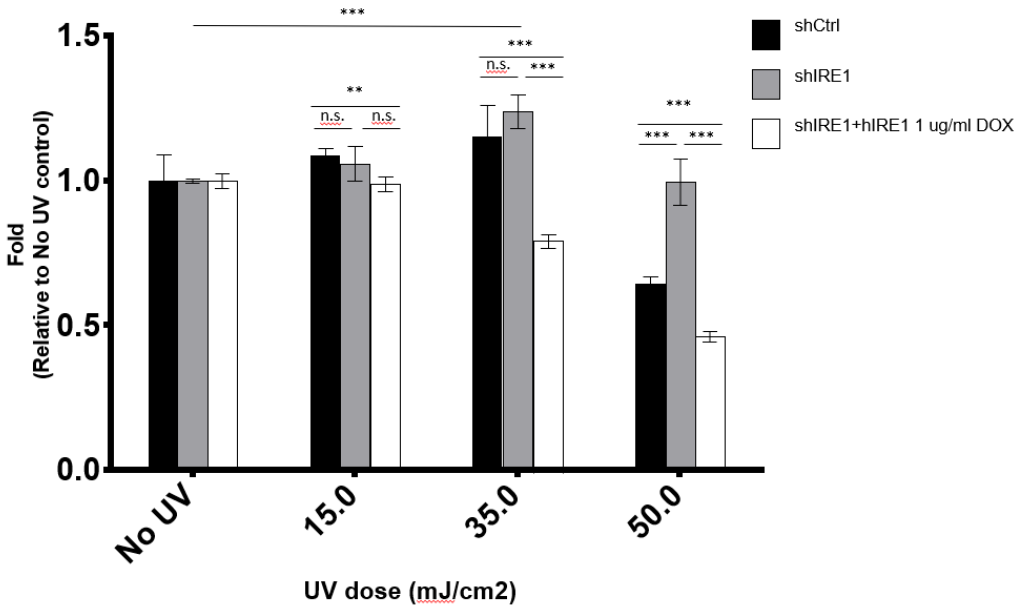

B.

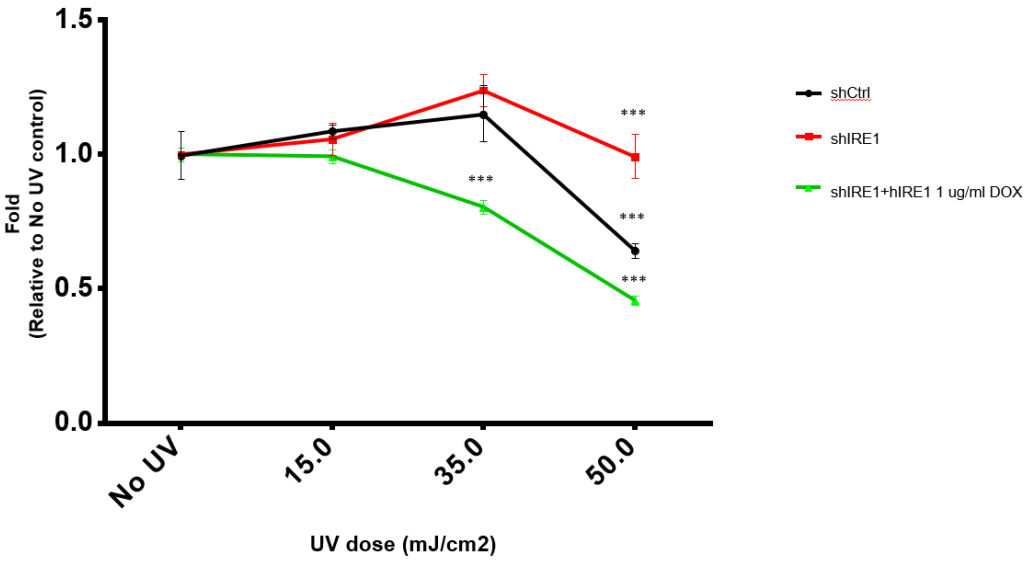

(A) MTT cell viability assay 24 hours post-UVB irradiation for each N-TERT cell line (n = 6 per line per dose) normalized to No UV control. n.s. = "no significance", ** = "p < 0.01", * = "p < 0.001". (B) Results from MTT assay displayed as a line graph for trend determination.**

3.7 p53 knockdown via siRNA leads to increased N-TERT cell death in response to acute UVB irradiation

After assessing how IRE1α expression affects UVB sensitivity of skin cells with either wildtype of mutant p53 expression, we subsequently wanted to investigate how loss of p53 expression affected UVB sensitivity of skin cells. To examine this, an additional UVB dose-response MTT cell viability assay was performed on N-TERT cell lines, using siRNA transfection to knockdown p53 expression. IRE1α control and knockdown N-TERT cell lines were transfected with either control or p53 siRNA, generating control and p53 knockdown models, respectively. After siRNA transfection, each cell type was irradiated with doses of 35.0 mJ/cm^2, 50.0 mJ/cm^2, and 65.0 mJ/cm^2 of UVB and no UV control, as was performed in the previous N-TERT UVB dose-response experiment. Absorbance measurements were taken 32 hours post-UVB irradiation, and measurements for cell types were normalized to their no UV control.

From Figure 7, p53 knockdown in N-TERT cells with IRE1α control expression resulted in significantly increased cell death at 65.0 mJ/cm^2 of UVB compared to wildtype p53 expression. Similarly, Figure 7 shows that p53 knockdown in N-TERT cells with IRE1α knockdown also yielded significantly increased cell death at 65.0 mJ/cm^2 of UVB compared to wildtype p53 expression. Comparing the lines with wildtype p53 expression, IRE1α knockdown in N-TERT cells yielded significantly decreased cell death compared to IRE1α control, as was seen in the previous N-TERT UVB dose-response experiment. Comparing the lines with knockdown p53, IRE1α knockdown in N-TERT cells again led to significantly decreased cell death compared to IRE1α control. Altogether, these results show that p53 knockdown leads to increased UVB sensitivity in N-TERT cells at high doses of UVB irradiation.

Figure 7. N-TERT cells MTT viability assay following siRNA transfection and UVB irradiation

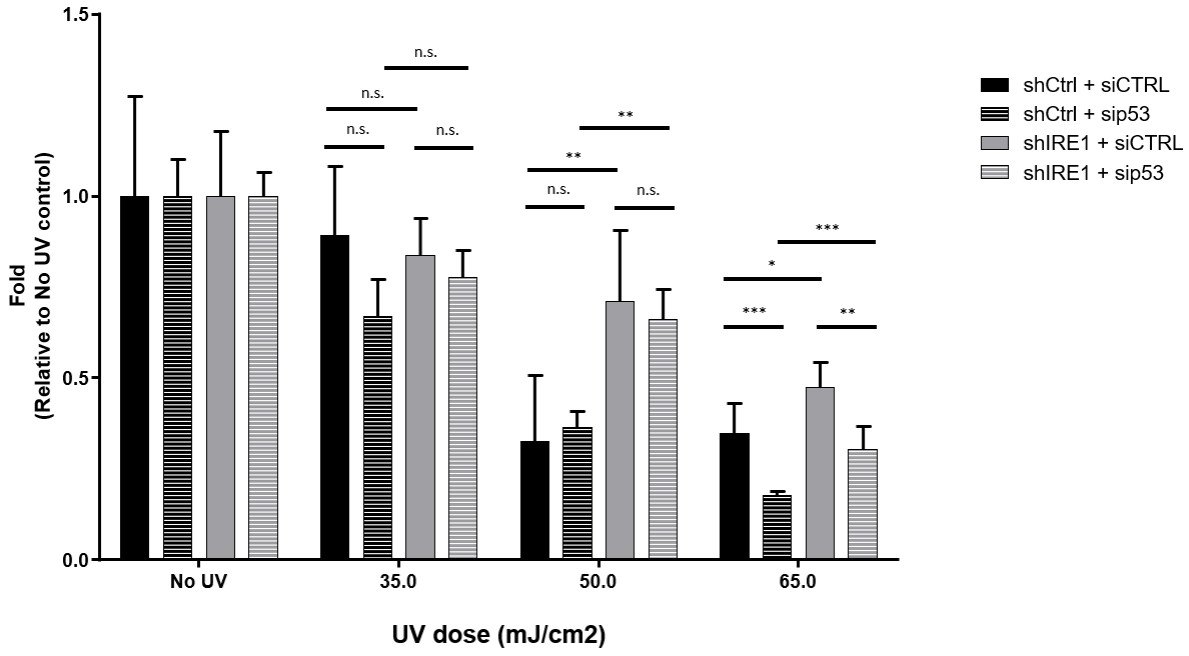

MTT cell viability assay 32 hours post-UVB irradiation for each N-TERT cell line (n = 6 per line per dose) normalized to No UV control. n.s. = "no significance", * = "$p < 0.05$", ** = "$p < 0.01$", * = "$p < 0.001$".**

Chapter 4

Discussion

4.1 Overview

UVB radiation remains a key area of cancer research as it is the most significant environmental risk factor for skin cancer development (1). UPR processes, mediated in part by IRE1α, may significantly influence skin cell sensitivity to acute UVB exposure by regulating responses to UV-induced influx of misfolded proteins in the ER (23). Additionally, key tumor suppressor proteins such as p53 also dictate the fate of UVB-exposed cells, sensing DNA damage to regulate UV-induced DDR pathways which result in apoptosis or cell cycle arrest and repair (46). By utilizing immortalized human keratinocytes with varying p53 and IRE1α expression levels, an effective *in vitro* model for assessing protein expression on the UV-induced DDR of skin cells, posing implications for responses of skin cancer.

The main goal of this thesis was to investigate how various cellular responses to acute UVB exposure differed in skin cell lines with manipulated IRE1α and p53 expression, linking responses of the UPR to the UV-induced DDR. HaCaT cells were employed as an effective model for skin cells possessing a mutational spectrum of p53 consistent with UV-induced DNA damage (52). In contrast, N-TERT cells were used as a skin cell model expressing wildtype p53 (54). Three different cell lines with varying levels of IRE1α expression were generated via lentivirus transduction for both HaCaT and N-TERT cell types: shIRE1α (knockdown), shIRE1α + hIRE1α (dox-inducible overexpression), and shCtrl (control). To mimic the effects of UVB irradiation on these cells, a CL-1000 Ultraviolet crosslinker was used to irradiate cells with acute doses of UVB radiation. Cellular responses were assessed, including cell viability via MTT

assay, apoptosis marker cleaved Caspase-3 via cell staining, DNA damage marker γH2AX via immunofluorescence, and basal calcium levels via cell staining.

After UV-induced DNA damage, cancer cells continue to survive and proliferate. As previously mentioned, tumor suppressor protein p53 is the most commonly mutated gene found among human cancer cells, especially in skin cancer (35). Understanding the role of IRE1α expression in affecting how cells with varying p53 expression (mutant, knockdown, or wildtype) survive after acute UVB irradiation may give helpful information into how IRE1α functions in the UV-induced DDR of cancer cells vs normal skin cells. 32 hours after UVB irradiation of HaCaT cells, IRE1α knockdown cells exhibited significantly increased cell death at all tested doses of acute UVB radiation compared to control, indicating that IRE1α knockdown leads to increased UVB sensitivity in mutant p53 skin cells (Figure 1A). Simultaneously, hIRE1α overexpression rescued HaCaT cells from death following UVB irradiation compared to control, indicated by increased cell viability of hIRE1α overexpression cells at all tested doses of acute UVB radiation compared to control (Figure 1A). Surprisingly, the effect of IRE1α expression on UVB-induced sensitization was reversed in N-TERT cells as IRE1α knockdown yielded significantly decreased cell death following 50.0 mJ/cm^2 of UVB radiation compared to control (Figure 6A). When p53 was silenced with siRNA in N-TERT cells, both IRE1α knockdown and control lines exhibited increased cell death compared to wildtype p53 expression (Figure 7). These results indicate that IRE1α knockdown and mutant p53 expression results in a synergistic loss of DNA repair functionality, leading to increased cell death following UVB irradiation. In contrast, IRE1α knockdown in wildtype p53 cells yielded decreased cell death following UVB irradiation, indicating a compensatory effect of wildtype p53 to sustain cell survival when IRE1α is knocked down. In the context of skin cancers where p53 mutations are common, IRE1α

knockdown may increase cell death and promote apoptosis, thus stopping tumorigenesis as UV-damaged cells die off. This effect is not seen when p53 is completely inactivated, as evidenced by increased cell viability of IRE1α knockdown cells with silenced p53 compared to wildtype p53. Therefore, the synergistic sensitization to acute UVB exposure of skin cells with mutant p53 and IRE1α knockdown is specific to the UV-induced mutational spectrum of p53 in HaCaT cells and is not specific to total loss-of-function p53 mutation. In total, the unique combination of p53 and IRE1α expression levels dictates survival of skin cells following acute UVB exposure.

Furthermore, an understanding of the specific responses of mutant p53 cells with varying IRE1α expression to UVB irradiation poses critical implications for skin cancer. By testing for cellular markers of apoptosis (cleaved Caspase-3) and DNA damage (γH2AX), a better understanding may be discovered for how IRE1α expression affects the UV-induced DDR of mutant-p53 skin cancer cells. After UVB irradiation, IRE1α knockdown HaCaT cells exhibited increased cleaved Caspase-3 levels and decreased γH2AX levels compared to control and hIRE1α overexpression (Figure 3A, Figure 5A). These results indicate that IRE1α knockdown of mutant p53 skin cells leads to increased apoptosis with increased levels of cleaved Caspase-3 and decreased capacity to survey and correct DNA damage with decreased levels of γH2AX. Taken together with previous MTT results, IRE1α knockdown in mutant p53 skin cells leads to increased sensitivity to acute doses of UVB radiation and decreased capacity for initiation of the DDR.

As noted previously, altered calcium homeostasis is a typical phenomenon in ER stress (17). Increased intracellular calcium concentration may relate to decreased ability to regulate calcium homeostasis upon cellular stresses, such as exposure to UV radiation. After knockdown of IRE1α in mutant-p53 HaCaT cells, cells exhibited a basal increased intracellular calcium

concentration compared to control and hIRE1α overexpression models (Figure 4A). From this, IRE1α knockdown in mutant-p53 skin cells leads to impaired calcium efflux, decreasing ability to regulate the response to ER stress and the UVB-induced DNA damage.

In conclusion, these experiments provide further evidence supporting a link between the UPR and the UV-induced DDR involving IRE1α, additionally highlighting a novel importance for mutation of tumor suppressor protein p53 in this process. IRE1α knockdown resulted in increased cell death and decreased ability to respond to UV-induced DNA damage for mutant-p53 skin cells. With respect to skin cancer and mutant-p53 cancers, this data provides meaningful insight into the sensitization of skin cells to UVB, thus identifying IRE1α and its downstream effectors as potential areas of inquiry for developing anti-cancer therapeutics.

4.2 Future Experiments

Further experiments could be conducted to better understand the relationship between the UPR and tumor suppressor p53 in skin cancer. First, additional molecules involved in the DDR and ER stress should be investigated after UVB irradiation of keratinocytes with varying IRE1α and p53 expression. Transforming growth factor beta 1 (TGFβ1), a key cytokine that regulates inflammatory responses and the cell cycle, has been observed to play a tumor-promoting role in UVB-induced skin cancer (56). Understanding how TGFβ1 functions in the UVB-induced DDR of cells with different levels of IRE1α and p53 expression could yield valuable insight into UV-induced tumorigenesis of mutant p53 skin cancers. To do this, HaCaT and N-TERT cell lines would be treated with doses of TGFβ1 prior to UVB irradiation. These cells would then be

assessed for cell viability or expression of various ER stress and DDR markers to determine responses to UVB irradiation caused from TGFβ1.

Also, p53 activation and cell cycle arrest has been observed to be triggered by the PERK-dependent functions of the UPR (57). Investigating how PERK and its downstream regulator eIF2α affects the UVB-induced DDR of skin cells *in vitro* may therefore provide useful information into the mechanisms of skin cancer. In examining the role of PERK in the UVB-induced DDR, future experiments may also study how RNA Polymerase II Associated Protein 2 (RPAP2), a phosphatase activated by PERK that reverses IRE1α phosphorylation, affects the UVB-induced DDR with respect to p53 expression. Potential experiments could involve manipulating PERK or RPAP2 expression before UVB irradiation of HaCaT and N-TERT cell lines, later measuring specific DDR and apoptosis markers to determine this effect. Results from these UVB *in vitro* experiments may give novel information about potential mechanisms for UVB sensitivity and UVB-induced tumorigenesis in keratinocytes, providing potential direction for therapeutic targets against cancer.

Lastly, future experiments may attempt to represent the skin tumor microenvironment more accurately through the use of spheroid cell cultures. By growing cells in 3D spheroids instead of conventional 2D cell cultures, generated models will more closely resemble *in vivo* and clinical results as protein and gene expression profiles of spheroids are more similar to real-life cells in the body (59). An effective spheroid model for melanoma has already been tested for future use in therapeutic development (60). Additionally, keratinocyte cell cultures are capable of forming spheroids, including HaCaT cells (61). Through the use of human keratinocyte spheroids, UVB irradiation experiments could be conducted to more accurately predict the effects of IRE1α and p53 in UVB sensitization of human skin cells.

BIBLIOGRAPHY

1. Guy, G.P., Machlin, S.R., Ekwueme, D.U., & Yabroff, K.R. (2015). Prevalence and Costs of Skin Cancer Treatment in the U.S., 2002–2006 and 2007–2011. *Am J Prev Med*, 48(2): 183-187. [PubMed: 25442229]
2. Leiter, U., & Garbe, C. (2008). Epidemiology of melanoma and nonmelanoma skin cancer--the role of sunlight. *Advances in experimental medicine and biology*, 624: 89–103. [PubMed: 18348450]
3. Lapouge, G., Youssef, K. K., Vokaer, B., Achouri, Y., Michaux, C., Sotiropoulou, P. A., & Blanpain, C. (2011). Identifying the cellular origin of squamous skin tumors. *Proceedings of the National Academy of Sciences of the United States of America*, 108(18): 7431–7436. [PubMed: 21502497]
4. Tan, S. T., Ghaznawie, M., Heenan, P. J., & Dosan, R. (2018). Basal Cell Carcinoma Arises from Interfollicular Layer of Epidermis. *Journal of oncology*, 2018: 3098940. [PubMed: 30356421]
5. Fontanillas, P., Alipanahi, B., Furlotte, N.A. et al. (2021). Disease risk scores for skin cancers. *Nat Commun*, 12: 160. [PubMed: 33420020]
6. Saladi, R. N., & Persaud, A. N. (2005). The causes of skin cancer: a comprehensive review. *Drugs of today*, 41(1): 37–53. [PubMed: 15753968]
7. Bradford P. T. (2009). Skin cancer in skin of color. *Dermatology nursing*, 21(4): 170–178. [PubMed: 19691228]
8. Benjamin, C. L., & Ananthaswamy, H. N. (2007). p53 and the pathogenesis of skin cancer. *Toxicology and applied pharmacology*, 224(3), 241–248. [PubMed: 17270229]
9. Sykes, E. K., Mactier, S., & Christopherson, R. I. (2016). Melanoma and the Unfolded Protein Response. *Cancers*, 8(3): 30. [PubMed: 26927180]
10. Voeltz, G. K., Rolls, M. M., & Rapoport, T. A. (2002). Structural organization of the endoplasmic reticulum. *EMBO reports*, 3(10): 944–950. [PubMed: 1237027]
11. Schwarz, D. S., & Blower, M. D. (2016). The endoplasmic reticulum: structure, function and response to cellular signaling. *CMLS*, 73(1): 79–94. [PubMed: 26433683]
12. Mandon, E. C., Trueman, S. F., & Gilmore, R. (2013). Protein translocation across the rough endoplasmic reticulum. *Cold Spring Harbor perspectives in biology*, 5(2): a013342. [PubMed: 23251026]
13. Dudek, J., Pfeffer, S., Lee, P. H. et al. (2015). Protein transport into the human endoplasmic reticulum. *Journal of molecular biology*, 427(6 Pt A): 1159–1175. [PubMed: 24968227]
14. Braakman, I., & Hebert, D. N. (2013). Protein folding in the endoplasmic reticulum. Cold *Spring Harbor perspectives in biology*, 5(5): a013201. [PubMed: 23637286]
15. Rao, R. V., & Bredesen, D. E. (2004). Misfolded proteins, endoplasmic reticulum stress and neurodegeneration. *Current opinion in cell biology*, 16(6): 653–662. [PubMed: 15530777]
16. Oakes SA, Papa FR. (2015). The role of endoplasmic reticulum stress in human pathology. *Annu Rev Pathol*, 10: 173-94. [PubMed: 25387057]

17. Wang, M., Kaufman, R.J. (2016). Protein misfolding in the endoplasmic reticulum as a conduit to human disease. *Nature*, 529(7586): 326-35. [PubMed: 26791723]
18. Schröder, M., & Kaufman, R. J. (2005). ER stress and the unfolded protein response. *Mutation research*, 569(1-2): 29–63. [PubMed: 15603751]
19. Gorman, A. M., Healy, S. J., Jager, R. & Samali, A. (2012). Stress management at the ER: regulators of ER stress-induced apoptosis. *Pharmacol Ther*, 134(3): 306–316. [PubMed: 22387231]
20. Liu, C. Y., & Kaufman, R. J. (2003). The unfolded protein response. *Journal of cell science*, 116(Pt 10): 1861–1862. [PubMed: 12692187]
21. Hetz, C., Zhang, K., & Kaufman, R. J. (2020). Mechanisms, regulation and functions of the unfolded protein response. *Nature reviews molecular cell biology*, 21(8): 421–438. [PubMed: 32457508]
22. Hillary, R. F., & FitzGerald, U. (2018). A lifetime of stress: ATF6 in development and homeostasis. *Journal of biomedical science*, 25(1): 48. [PubMed: 29801500]
23. Merksamer, P. I., & Papa, F. R. (2010). The UPR and cell fate at a glance. *Journal of cell science*, 123(Pt 7): 1003–1006. [PubMed: 20332117]
24. Han, D., Lerner, A.G., Walle, L.V. et al. (2009). IRE1alpha kinase activation modes control alternate endoribonuclease outputs to determine divergent cell fates. *Cell*, 138(3): 562–575. [PubMed: 19665977]
25. Park, S. M., Kang, T. I., & So, J. S. (2021). Roles of XBP1s in Transcriptional Regulation of Target Genes. *Biomedicines*, 9(7): 791. [PubMed: 34356855]
26. Dufey, E., Bravo-San Pedro, J.M., Eggers, C. et al. (2020). Genotoxic stress triggers the activation of IRE1α-dependent RNA decay to modulate the DNA damage response. *Nat Commun*, 11: 2401. [PubMed: 32409639]
27. Urano, F., Wang, X., Bertolotti, A. et al. (2000). Coupling of stress in the ER to activation of JNK protein kinases by transmembrane protein kinase IRE1. *Science*, 287(5453): 664–666. [PubMed: 10650002]
28. Li, X., Zhang, K., & Li, Z. (2011). Unfolded protein response in cancer: the physician's perspective. *Journal of hematology & oncology*, 4: 8. [PubMed: 21345215]
29. Qu, L., Huang, S., Baltzis, D. et al. (2004). Endoplasmic reticulum stress induces p53 cytoplasmic localization and prevents p53-dependent apoptosis by a pathway involving glycogen synthase kinase-3beta. *Genes & development*, 18(3): 261–277. [PubMed: 14744935]
30. Zhou, B. B., & Elledge, S. J. (2000). The DNA damage response: putting checkpoints in perspective. *Nature*, 408(6811): 433–439. [PubMed: 11100718]
31. Lowndes, N. F., & Murguia, J. R. (2000). Sensing and responding to DNA damage. *Current opinion in genetics & development*, 10(1): 17–25. [PubMed: 10679395]
32. Mah, L. J., El-Osta, A., & Karagiannis, T. C. (2010). gammaH2AX: a sensitive molecular marker of DNA damage and repair. *Leukemia*, 24(4): 679–686. [PubMed: 20130602]
33. Hinds, P. W., & Weinberg, R. A. (1994). Tumor suppressor genes. *Current opinion in genetics & development*, 4(1): 135–141. [PubMed: 8193533]

34. Cadwell, C., & Zambetti, G. P. (2001). The effects of wild-type p53 tumor suppressor activity and mutant p53 gain-of-function on cell growth. *Gene*, 277(1-2): 15–30. [PubMed: 11602342]
35. Kato, S., Han, S. Y., Liu, W., Otsuka, K., Shibata, H., Kanamaru, R., & Ishioka, C. (2003). Understanding the function-structure and function-mutation relationships of p53 tumor suppressor protein by high-resolution missense mutation analysis. *Proceedings of the National Academy of Sciences of the United States of America*, 100(14): 8424–8429. [PubMed: 12826609]
36. Vogelstein, B., & Kinzler, K. W. (1992). p53 function and dysfunction. *Cell*, 70(4): 523–526. [PubMed: 1505019]
37. Whibley, C., Pharoah, P. D., & Hollstein, M. (2009). p53 polymorphisms: cancer implications. *Nature reviews. Cancer*, 9(2): 95–107. [PubMed: 19165225]
38. Harper, J. W., Adami, G. R., Wei, N., Keyomarsi, K., & Elledge, S. J. (1993). The p21 Cdk-interacting protein Cip1 is a potent inhibitor of G1 cyclin-dependent kinases. *Cell*, 75(4): 805–816. [PubMed: 8242751]
39. Ziegler, A. et al. (1994). Sunburn and p53 in the onset of skin cancer. *Nature*, 372(6508): 773-776. [PubMed: 7997263]
40. Oren, M., & Rotter, V. (2010). Mutant p53 gain-of-function in cancer. *Cold Spring Harbor perspectives in biology*, 2(2): a001107. [PubMed: 20182618]
41. Wang, Y.H. et al. (2020). Both DNA binding domains of p53 are required for its ultra-rapid recruitment to sites of UV damage. *bioRxiv*, pre-print. https://doi.org/10.1101/2020.02.09.938993.
42. de Gruijl F. R. (2000). Photocarcinogenesis: UVA vs UVB. *Methods in enzymology*, 319: 359–366. [PubMed: 10907526]
43. Drouin, R., & Therrien, J. P. (1997). UVB-induced cyclobutane pyrimidine dimer frequency correlates with skin cancer mutational hotspots in p53. *Photochemistry and photobiology*, 66(5): 719–726. [PubMed: 9383997]
44. You, Y. H., Lee, D. H., Yoon, J. H., Nakajima, S., Yasui, A., & Pfeifer, G. P. (2001). Cyclobutane pyrimidine dimers are responsible for the vast majority of mutations induced by UVB irradiation in mammalian cells. *The Journal of biological chemistry*, 276(48): 44688–44694. [PubMed: 11572873]
45. Verschooten, L., Declercq, L., & Garmyn, M. (2006). Adaptive response of the skin to UVB damage: role of the p53 protein. *International journal of cosmetic science*, 28(1): 1–7. [PubMed: 18492196]
46. Williams, A.B., & Schumacher, B. (2016). p53 in the DNA-Damage-Repair process. *Cold Spring Harb Perspect Med* 6(5): a026070. [PubMed: 27048304]
47. Shimizu, H., Banno, Y., Sumi, N., Naganawa, T., Kitajima, Y., & Nozawa, Y. (1999). Activation of p38 mitogen-activated protein kinase and caspases in UVB-induced apoptosis of human keratinocyte HaCaT cells. *The Journal of investigative dermatology*, 112(5): 769–774. [PubMed: 10233770]
48. Porter, A. G., & Jänicke, R. U. (1999). Emerging roles of caspase-3 in apoptosis. *Cell death and differentiation*, *6*(2): 99–104. [PubMed: 10200555]

49. Ananthaswamy, H. N., Loughlin, S. M., Cox, P., et al. (1997). Sunlight and skin cancer: inhibition of p53 mutations in UV-irradiated mouse skin by sunscreens. *Nat Med*, 3(5): 510-514. [PubMed: 9142118]
50. Mera, K., Kawahara, K., Tada, K., et al. (2010). ER signaling is activated to protect human HaCaT keratinocytes from ER stress induced by environmental doses of UVB. *Biochemical and biophysical research communications*, 397(2): 350–354. [PubMed: 20513357]
51. Son, J., Mogre, S., Chalmers, F. E., et al. (2021). The Endoplasmic Reticulum Stress Sensor IRE1α Regulates the UV DNA Repair Response through the Control of Intracellular Calcium Homeostasis. *The Journal of investigative dermatology*, S0022-202X(21)02508-2. Advance online publication. [PubMed: 34808241]
52. Lehman, T. A., Modali, R., Boukamp, P., et al. (1993). p53 mutations in human immortalized epithelial cell lines. *Carcinogenesis*, 14(5): 833–839. [PubMed: 8504475]
53. Colombo, I., Sangiovanni, E., Maggio, R., et al. (2017). HaCaT Cells as a Reliable In Vitro Differentiation Model to Dissect the Inflammatory/Repair Response of Human Keratinocytes. *Mediators of inflammation*, 2017: 7435621. [PubMed: 29391667]
54. Smits, J., Niehues, H., Rikken, G., van Vlijmen-Willems, I., van de Zande, G., Zeeuwen, P., Schalkwijk, J., & van den Bogaard, E. H. (2017). Immortalized N/TERT keratinocytes as an alternative cell source in 3D human epidermal models. *Scientific reports*, 7(1), 11838. [PubMed: 28928444]
55. Stockert, J. C., Blázquez-Castro, A., Cañete, M., et al. (2012). MTT assay for cell viability: Intracellular localization of the formazan product is in lipid droplets. *Acta histochemica*, 114(8): 785–796. [PubMed: 22341561]
56. Ravindran, A., Mohammed, J., Gunderson, A. J., Cui, X., & Glick, A. B. (2014). Tumor-promoting role of TGFβ1 signaling in ultraviolet B-induced skin carcinogenesis is associated with cutaneous inflammation and lymph node migration of dermal dendritic cells. *Carcinogenesis*, *35*(4): 959–966. [PubMed: 24363069]
57. Zhang, F., Hamanaka, R. B., Bobrovnikova-Marjon, E., Gordan, J. D., Dai, M. S., Lu, H., Simon, M. C., & Diehl, J. A. (2006). Ribosomal stress couples the unfolded protein response to p53-dependent cell cycle arrest. *The Journal of biological chemistry*, *281*(40): 30036–30045. [PubMed: 16893887]
58. Chang, T. K., Lawrence, D. A., Lu, M., Tan, J., Harnoss, J. M., Marsters, S. A., Liu, P., Sandoval, W., Martin, S. E., & Ashkenazi, A. (2018). Coordination between Two Branches of the Unfolded Protein Response Determines Apoptotic Cell Fate. *Molecular cell*, *71*(4): 629–636.e5. [PubMed: 30118681]
59. Katt, M. E., Placone, A. L., Wong, A. D., Xu, Z. S., & Searson, P. C. (2016). In Vitro Tumor Models: Advantages, Disadvantages, Variables, and Selecting the Right Platform. *Frontiers in bioengineering and biotechnology*, *4*: 12. [PubMed: 26904541]
60. Müller, I., & Kulms, D. (2018). A 3D Organotypic Melanoma Spheroid Skin Model. *Journal of visualized experiments : JoVE*, 135: 57500. [PubMed: 29863656]

61. Klicks, J., Maßlo, C., Kluth, A., Rudolf, R., & Hafner, M. (2019). A novel spheroid-based co-culture model mimics loss of keratinocyte differentiation, melanoma cell invasion, and drug-induced selection of ABCB5-expressing cells. BMC cancer, 19(1): 402. [PubMed: 31035967]

ACADEMIC VITA
JACK W. IBINSON

EDUCATION

The Pennsylvania State University, State College, PA
Schreyer Honors College, August 2018 – Present
Bachelor of Science in Immunology and Infectious Disease, **Minors in Biology and Statistics,** Class of 2022

RESEARCH

Undergraduate Researcher, *Dr. Adam Glick's Lab,* The Pennsylvania State University, January 2020 – Present

- Investigated role of IRE1α and p53 proteins in UVB-induced skin cancer *in vitro*
- Generated human knockdown cell lines via transduction with siRNA lentivirus for hypothesis-driven experiments
- Analyzed cell images and histology slides through QuPath bioimage software for graduate-level research projects

PUBLICATIONS

- Son, J., Mogre, S., Chalmers, F. E., Ibinson, J., Worrell, S., & Glick, A. B. (2021). The ER Stress Sensor IRE1α Regulates the UV DNA Repair Response Through Control of Intracellular Calcium Homeostasis. *The Journal of investigative dermatology*, S0022-202X(21)02508-2. Advance online publication. https://doi.org/10.1016/j.jid.2021.11.010.

AWARDS

Summer 2021 Erickson Discovery Grant

- Granted $3,500 of project funding for summer research towards undergraduate biomedical thesis

Spring 2021 Gamma Sigma Delta Research Exposition- 3rd Place Award in Animal Systems

- Earned recognition for excellence in undergraduate research

Fall 2020 Penn State College of Agricultural Sciences Undergraduate Research Award

- Awarded $2,000 of funding for project entitled: *The Role of IRE1α and p53 in HaCaT Keratinocyte Survivability Following UV-B Irradiation*

INVOLVEMENT

Penn State Chapter of Remote Area Medical (Penn State RAM), August 2018 – Present

- Leadership positions: Vice President, Secretary
- Assisted in providing free medical, dental, and vision care to over 2,000 total patients across 5 clinics in underserved communities
- Oversaw all operations for 9-person executive board to ensure strong communication and collaboration
- Organized hospitality, travel, and lodging arrangements for 29 students on clinic trip in Bellmont, NY

ServeState: Students for Philanthropy, August 2018 – Present

- Leadership positions: Service Coordinator, Marketing Chair, Mentorship Guide
- Participated in community service and philanthropic efforts to directly benefit the State College Community
- Arranged weekend-long service retreat for 60 club members to promote teambuilding and volunteerism
- Awarded Club Humanitarian Award for Fall 2018, Fall 2019
- Received Club Service Award for Fall 2019

Penn State Department of Chemistry Learning Assistant (LA), January – May 2021

- Served as LA for Organic Chemistry I course to effectively educate class of 320 students
- Led 2 weekly workshop sessions and held office hours to facilitate class engagement and active learning

WORK EXPERIENCE

Laborer, June 2015 – August 2018, May 2019 – August 2019, May 2020 – August 2020

3 Sons Construction, Pittsburgh, PA

- Assisted in construction and repair of various private residential and public housing properties
- Utilized critical thinking and organization skills to efficiently meet tight deadlines during COVID-19 pandemic

SERVICE EXPERIENCE

Completed 70 hours of community service yearly

- Mount Nittany Medical Center, Remote Area Medical clinics, Krislund Camp and Conference Center, The Arboretum at Penn State, Penn State LifeLink, Shaver's Creek Environmental Center, RE Farm Cafe